AD-A183 754 SHAPE FROM PROJECTING A STRIPE PATTERN(U) MARYLAND UNIV 1/1
COLLEGE PARK CENTER FOR AUTOMATION RESEARCH
M ASADA ET AL. JAN 87 CAR-TR-263 ETL-0453
UNCLASSIFIED DACA76-84-C-0004 F/G 14/5 NL

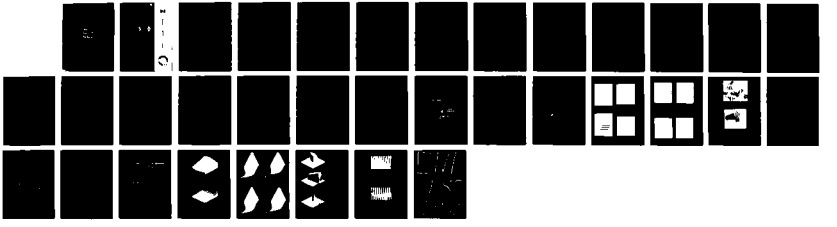

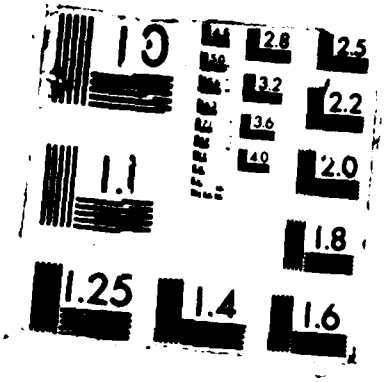
1.0
1.1
2.8
3.2
3.6
4.0
2.5
2.2
2.0
1.8
1.25
1.4
1.6

ETL-0453

AD-A183 754

Shape from projecting a stripe pattern

Minoru Asada
Saburo Tsuji

Center for Automation Research
University of Maryland
College Park, MD 20742-3411

January 1987

Prepared for
U.S. ARMY CORPS OF ENGINEERS
ENGINEER TOPOGRAPHIC LABORATORIES
FORT BELVOIR, VIRGINIA 22060-5546

E T L

UNCLASSIFIED
SECURITY CLASSIFICATION OF THIS PAGE

REPORT DOCUMENTATION PAGE

Form Approved
OMB No 0704-0188
Exp Date Jun 30, 1986

1a. REPORT SECURITY CLASSIFICATION UNCLASSIFIED	1b. RESTRICTIVE MARKINGS N/A
2a. SECURITY CLASSIFICATION AUTHORITY N/A	3. DISTRIBUTION/AVAILABILITY OF REPORT Approved for public release; distribution unlimited
2b. DECLASSIFICATION/DOWNGRADING SCHEDULE N/A	
4. PERFORMING ORGANIZATION REPORT NUMBER(S) CAR-TR-263 CS-TR-1773	5. MONITORING ORGANIZATION REPORT NUMBER(S) ETL-0453
6a. NAME OF PERFORMING ORGANIZATION University of Maryland 6b. OFFICE SYMBOL (If applicable) N/A	7a. NAME OF MONITORING ORGANIZATION Army Engineer Topographic Laboratories
6c. ADDRESS (City, State, and ZIP Code) Center for Automation Research College Park, MD 20742-3411	7b. ADDRESS (City, State, and ZIP Code) Fort Belvoir, VA 22060
8a. NAME OF FUNDING/SPONSORING ORGANIZATION Defense Advanced Research Projects Agency 8b. OFFICE SYMBOL (If applicable)	9. PROCUREMENT INSTRUMENT IDENTIFICATION NUMBER DACA76-84-C-0004
8c. ADDRESS (City, State, and ZIP Code) 1400 Wilson Boulevard Arlington, VA 22209	10. SOURCE OF FUNDING NUMBERS PROGRAM ELEMENT NO. / PROJECT NO. / TASK NO. / WORK UNIT ACCESSION NO

11. TITLE (Include Security Classification)

Shape from Projecting a Stripe Pattern

12. PERSONAL AUTHOR(S)

Minoru Asada and Saburo Tsuji

13a. TYPE OF REPORT	13b. TIME COVERED	14. DATE OF REPORT (Year, Month, Day)	15. PAGE COUNT
Technical	FROM _____ TO N/A	January 1987	33

16. SUPPLEMENTARY NOTATION

17. COSATI CODES			18. SUBJECT TERMS (Continue on reverse if necessary and identify by block number)
FIELD	GROUP	SUB-GROUP	

19. ABSTRACT (Continue on reverse if necessary and identify by block number)

This paper presents a simple method which determines the shape of an object by projecting a stripe pattern on to it. Assuming orthographical projection as a camera model and parallel light projection of the stripe pattern, the method obtains a 2(1/2)D representation of objects by estimating surface normals from the slopes and intervals of the stripes in the image. The 2(1/2)D image is further divided into planar or singly curved surfaces by examining the distribution of the surface normals in gradient space. Some applications and evaluation of the error in surface orientation are described.

20 DISTRIBUTION/AVAILABILITY OF ABSTRACT ☐ UNCLASSIFIED/UNLIMITED ☒ SAME AS RPT ☐ DTIC USERS	21 ABSTRACT SECURITY CLASSIFICATION UNCLASSIFIED
22a. NAME OF RESPONSIBLE INDIVIDUAL	22b TELEPHONE (Include Area Code) / 22c OFFICE SYMBOL

DD FORM 1473, 84 MAR

83 APR edition may be used until exhausted
All other editions are obsolete

SECURITY CLASSIFICATION OF THIS PAGE
UNCLASSIFIED

1. INTRODUCTION

Acquisition of scene properties such as depth and surface orientation is one of the key problems in both computer vision and robot vision. Many researchers have explored methods of obtaining these properties from 2-D imagery using physical constraints on the light source, object class, or surface properties of the object, or using multiple views [1]. Stereo vision is one of the methods which obtains depth information using the disparity between the projected positions of feature points in two views [2]. Finding the correspondence between feature points in the two stereo images, however, is the most important and difficult problem in stereo vision [3,4]. Structured lighting methods are often used for quick acquisition of range information [5–7]. These methods utilize a projection of a regular pattern of light instead of one of the two stereo cameras in order to encode 3-D information; therefore, establishing a correspondence between the stripes in the image and the light stripes in scene is also necessary when a stripe pattern is used. Abrupt changes in depth are the main concern in these methods because they disable the labeling of the stripe pattern. Although scanning a light stripe through a slit has been developed to avoid the correspondence problem, it is expensive and requires a long time for image acquisition [8].

We have proposed a new method which determines the surface orientation of each point on an object, instead of providing depth information, by projecting a stripe pattern without requiring correspondence between the stripe pattern in the image and that in the scene [9,10]. The image acquisition system is arranged such that all light stripes in scene are almost parallel and the projection from

scene to image is orthographic. Thus, we can obtain a 2(1/2)D representation of the scene by estimating the surface normals from the slopes and intervals of the stripes in the image. The 2(1/2)D image is further segmented into planar or singly curved surfaces by finding and examining clusters of the surface normals in gradient space. Although the estimate of each surface normal is somewhat inaccurate, we can obtain much better estimates of the geometrical parameters of the surfaces by utilizing the continuity of each surface.

Sugihara [11] proposed a method similar to our approach which infers local surface orientation using the distortion of a known pattern projected on the object surface from a structured light source. The projected texel on the object surface is detected and the distortion from the regular pattern is measured in order to estimate the surface orientation. Wang et al. [12] also proposed a method which determines local surface orientation of objects using grid coding. They use two orthogonal grid patterns, measure their orientations in the image, and then estimate surface orientation at the grid junctions. Adopting a stripe pattern as the structured lighting provides us the following advantages over these methods. The computation time to infer local surface orientation is shorter since our method need not find any texel patterns or grid junctions in the image, but need only locate stripe edge points so that the slopes and intervals of the stripes in the image can be easily measured. Many more surface normals are obtained along the detected stripe edge points. The richness of these points enables us to segment the image into meaningful regions corresponding to planar and singly curved surfaces and to refine the surface parameters of these regions using longer

stripes and wider intervals between the stripes in the image.

In this paper, we show some applications of our method and evaluate the error in surface orientation introduced by the orthographical projection. Evaluation of this error is important in a practical sense. The relation among the error in orientation, the focal length of the camera, the source direction and the stripe width is investigated. The following remarks can be made, assuming that the location of the stripe edge points is precisely estimated.

(1) Obviously, the larger the focal length, the smaller the error in orientation.

(2) The stripe width does not have much effect on the estimated surface orientation.

(3) The source direction determines the observable and measurable field of surface orientation. Outside this area, estimation of the surface normals is impossible.

2. METHODS

2.1 Determining Surface Orientation

Surface orientation is determined locally from the slopes and spacings of the stripes in the image. Fig. 1 shows the geometrical relations among light planes and an object plane in the camera-centered coordinate system. We define the equations of two light planes LP_1 and LP_2 parallel to each other, and of an object plane OP on which a stripe pattern is projected, as

$$LP_1 : P_s X + Q_s Y + Z = D_1,$$

$$LP_2 : P_s X + Q_s Y + Z = D_2,$$

and

$$OP : P_o X + Q_o Y + Z = C,$$

where (P_s, Q_s) represents the orientation of the light planes of the stripe pattern projection and (P_o, Q_o) is the surface orientation to be obtained. The object plane OP and the light plane LP_1 (LP_2) intersect in a line L_1 (L_2). The projections of lines L_1 and L_2 onto the image plane (the x-y plane) are denoted by l_1 and l_2, respectively. The slopes of these lines ($\tan\theta$) and the distance between them (Δx) in the x-axis direction are easily measured in the image since we assume orthographic projection. The geometrical relation among these variables leads to the following equations:

$$\tan\theta = -\frac{P_s - P_o}{Q_s - Q_o}, \quad \Delta x = \frac{D_2 - D_1}{P_s - P_o}.$$

From these equations we get

$$P_o = P_s - \frac{D_2 - D_1}{\Delta x} \text{ and } Q_o = \frac{D_2 - D_1}{\tan(\theta) * \Delta x} + Q_s. \tag{2.1}$$

That is, the surface orientation (P_o, Q_o) of a point on an object can be locally calculated from the slope ($\tan\theta$) and interval (Δx) of a stripe in the image.

2.2 Estimating the Locations of Stripe Edge Points

The accuracy of estimated surface orientation depends on the measurement of the slopes and spacings of the stripes in the image, which are calculated from stripe edge points. Therefore, precise estimation of edge location is necessary in our method. In order to reduce the effect of digitizing error, the location of an edge point is estimated to sub-pixel accuracy by using the Linear Mixing Model

[13] of intensity around a boundary between dark and bright regions. Figs. 2 show the process of stripe edge location. Fig. 2(a) indicates a linear mixing model of intensity in row $I(x)$, at the center of which a stripe edge exists; x_c is the location of the stripe edge to be obtained. The edge strength $G(x)$ in Fig. 2(c) is obtained by applying a rectangle operator as in Fig. 2(b) to the $I(x)$ in Fig. 2(a). The following equation gives the edge position x_c as the centroid of the peak region in which $G(x)$ is greater than a pre-determined threshold:

$$x_c = \frac{\sum_i^j G(x) * x}{\sum_i^j G(x)}.$$

In the experiments described later, the input image is digitized into 256 by 256 pixels, 256 gray levels per pixel, and edge location is represented to two decimal places.

Next, we fit a line segment to each of seven successive edge points. Those segments whose fitting error exceeds the threshold are discarded as discontinuous boundaries. Thus, the slopes and intervals of the stripes in the image are obtained from the gradients and distances between the fitted line segments.

2.3 Registration of Stripe Pattern

In order to determine surface orientation, the first step is to know the parameters of the stripe pattern, that is, the orientation of the light plane (P_s, Q_s) and the width of a stripe (D_2–D_1) with respect to the camera-centered coordinate system. We determine them with a plaster sphere as follows:

(1) Input an image of the plaster sphere without a stripe pattern projection and determine the location of the sphere in the image from its contour.

(2) Input another image of the same sphere at the same position with a stripe pattern projected on it.

(3) Apply the method in Section 2.2 to the input image in step (2) in order to measure the slopes and intervals of the stripes, and determine the stripe parameters by the least squares method using all the surface orientations calculated from the image position and the sphere location in step (1).

Fig. 3(a) shows the surface orientations used for estimation of the stripe parameters, and Fig. 3(b) shows the result of inferring surface orientations from the estimated stripe parameters. The distance between the camera and objects is about 4m (4 degrees of visual angle) and the angle between the optical axis and the light source direction is approximately 15 degrees. The standard deviations of the estimated parameters are 0.3 degrees in P_s, 1.1 degrees in Q_s and 1.25 pixels in (D_2-D_1), which equals 6% of the stripe width. With a more perfect sphere, the standard deviations would be decreased since the plaster sphere used is not a perfectly true one.

3. APPLICATIONS OF THE METHOD

3.1 Static Scene

Finding a known object and determining its attitude are important and frequently occurring tasks in both computer vision and robot vision. In this section, the 2(1/2)D image of surface normals obtained by our method is utilized for these

applications.

Many objects observed in daily life consist of planar or singly curved surfaces the shapes of which can be a key feature for discrimination of such objects as polyhedra, cylindrical objects and cone-like objects. Therefore, we first map the obtained surface normals onto gradient space in order to segment the 2(1/2)D image into planar or singly curved surfaces. Since it is difficult to extract the exact shapes of planar regions from an image with a projected stripe pattern, we prepare a segmented image consisting of regions obtained by applying the Sobel operator to the grey-tone image of the same scene with ordinary lighting. The surface normals to a plane make a cluster in gradient space. By mapping them from gradient space into the 2(1/2)D image and the pre-segmented image, we obtain the planar region. Its orientation is precisely estimated by calculating again using longer line segments and wider intervals. We can easily obtain frontal views of planar regions by rotating the planes so that they are parallel to the image plane. Simple shape matching of planar regions to known objects helps us determine which object is present, and its orientation.

Figs. 4(a) and (b) show an input image of a cube with a projected stripe pattern and the corresponding edge picture. Figs. 4(c) and (d) show the needle map of surface normals obtained by our method and the distribution map of the normals in gradient space. There are three clusters in Fig. 4(d) which correspond to three regions A, B, and C in the presegmented image Fig. 4(e). The frontal shapes of regions A, B and C are shown in Fig. 4(f), (g) and (h), respectively. Each of the three angles between planes A, B and C is approximately 90 degrees.

Other results can be seen in [8].

3.2 Dynamic Scene

Determining 3-D motion parameters in a time-varying scene is a current problem in computer vision. Interesting theories have been presented to estimate the 3-D motions of objects from a sequence of images taken by a camera [14–16]. Assuming the rigidity of objects, these theories analyze changes in the geometry of an object's images in consecutive frames to obtain 3-D motion cues. The results of applying these theories to real scenes, however, are very sensitive to noise and unsatisfactory in most cases. Therefore, a reliable method to obtain scene features from each frame in an image sequence is necessary.

We use the 2(1/2)D image of surface normals obtained by our method as a guide to find the correspondence between frames in dynamic scene analysis. Determining the 3-D motion parameters of an object is straightforward, given the correspondence of scene features between consecutive frames.

First, we map the obtained surface normals onto gradient space in order to segment the 2(1/2)D image into planar or singly curved surfaces. The surface normals to a plane make a cluster in gradient space as mentioned in Section 3.1. By reverse-mapping them from gradient space into the 2(1/2)D image, we obtain the planar region. In this case, the shape of each region is not extracted exactly because we cannot prepare the pre-segmented image used in the previous section due to the motions of the objects. The surface normals to a singly curved surface, for example a cylindrical surface, make a line-like cluster in gradient space.

The line parameters obtained by fitting a line to the cluster give us the orientation of the generating line of the cylindrical surface. Similar refinement of the surface parameters is performed.

Figs. 5(a) and (b) show the fifth frame of the sequence of input images and the moving objects in the fifth frame, respectively. A cylinder and a wedge are moving above a stack of blocks. The process of extracting the moving objects is described in detail in [9]. Fig. 6(a) shows the sampled surface normals on the moving object in the fifth frame. In Fig. 6(b), a histogram of these surface normals in gradient space is shown. Since the lower surface of the wedge is parallel to the generating line of the cylindrical surface, the cluster corresponding to it is merged into a line-like cluster (see Fig. 6(b)). Therefore, we cannot detect the lower surface of the wedge in gradient space at first. The line-like cluster, however, is segmented into two surfaces by examining the surface continuity on the 2(1/2)D image. Fig. 7 shows the result of the segmentation.

Since each 2(1/2)D image is segmented into planar or singly curved surfaces, it is easy to find the correspondences between these surfaces in consecutive frames. Finally, we determine the motion parameters from the surface properties obtained for each frame by assuming rigidity of the objects [15]. Fig. 8 shows the changes of surface orientation in consecutive frames and the rotation axis between two consecutive frames on the Gaussian sphere. Small circles without an axis indicate surface orientations (surface normal for planar regions, and orientation of generating line for cylindrical surfaces). Axes 1 and 2 represent the orientation of the rotation axes between the second and fifth frames and the fifth

and eighth frames, respectively. The angles between every pair of regions in each frame are shown in Table 1. The small change in these angles between frames shows the validity of our method.

4. ERROR ANALYSIS

In the experiments in Section 3, we used about twenty times the object size as the distance between the camera (or the projector) and the object in order to reduce the approximation error involved in the orthographical projection that was used. Such an image acquisition system is more difficult to set up when the object size is much larger or the experimental room is too small for such a long distance. Therefore, investigation of the relations among the surface orientation estimated by assuming orthographical projection, the focal length, the source direction and the stripe width is both interesting and meaningful for the use of the method in many practical applications.

Therefore, let us consider the effect on the surface orientation introduced by approximating central projection by orthographical projection. For simplicity and without loss of generality, we assume that Q_s, the gradient of the light plane in the y-axis direction, equals zero. Fig. 9 shows the top view of the image acquisition system in the central projection system. In order to compare with the estimate based on assuming orthographical projection, we choose the virtual image plane so that the observed point O_i on the object lies on it. The virtual slide plane through which the light source can project a stripe pattern in the scene is set at the virtual image center and perpendicular to the source direction.

The equations and coordinates in the (z,x)-coordinate system are given in Fig. 9. The light through the i-th slit S_i on the virtual slide plane intersects the object plane at the point O_i whose x-coordinate is x_i in the virtual image plane.

First, we consider the effect on P_o, which can be determined from the interval between the stripes in image. The error angle E_p between the true orientation P_o and the estimated orientation is

$$E_p = \tan^{-1}(P_o) - \frac{\tan^{-1}(P_l)+\tan^{-1}(P_r)}{2} \tag{4.1}$$

where P_l and P_r are obtained by substituting the left interval $(x_i - x_{i-1})$ and the right interval $(x_{i+1} - x_i)$ instead of Δx into eq. (2.1), respectively. We show by simulation how E_p would change with various parameters (the orientation of the object plane P_o, the image position x_i, the focal length f, the source direction P_s and the stripe width $(D_2 - D_1)$) since extracting the relation between E_p and the other parameters analytically from eq. (4.1) seems difficult. In the results of the following simulations <1–4>, we assume that the edge locations of the stripes in the image are obtained precisely.

<1> *P_o vs. $x_i(f)$* : First, we estimate the error angle E_p using almost the same parameters of focal length, source direction and stripe width as in the experiment in Section 3. The image size is 256 by 256 pixels and the equivalent focal length f is 3500 pixels, which means about 4 degrees of visual angle. The incident angle between the optical axis and the source direction is about 15 degrees ($P_s = 3.68$) and the stripe width $(D_2 - D_1)$ is 11 pixels. Fig. 10 shows the estimated value of E_p at various image positions $(-127 < x < 128)$ and surface orientations

($-63^\circ < \tan^{-1}(P_o) < 64^\circ$). From this figure, we can deduce the following conclusions:

* The error angle E_p is nearly proportional to the image position. In other words, we need n times the focal length in order to reduce the error angle by a factor of $\frac{1}{n}$.

* The sign of E_p tells us that the orientation is overestimated if the image position $x > 0$ and underestimated if $x < 0$.

* Although the orientation at which E_p has its maximal value depends on the source direction as described in <3>, the maximal value is independent of it. In this case, the maximal E_p (in short $E_p^{\max}$) is 4 degrees at the leftmost (or rightmost) position in the image when $\tan^{-1}(P_o) = -20.0^\circ$.

<2> (D_2-D_1) : *The change of* $E_p^{\max}$ *with stripe width* is shown in Table 1 where the other parameters are the same as in <1>. From this table, the stripe width seems not to have very much effect on $E_p^{\max}$. However, there is a trade-off problem between the accuracy and the number of surface normals, because accurate detection of stripe edge position is difficult in practice. In order to increase the accuracy of the surface normal at each point, we have to project a wider stripe pattern, and then we obtain a smaller number of surface normals. If we project a denser stripe pattern, the accuracy of the surface normal at each point decreases. The optimal stripe width depends on the shape of the object, the albedo of the surface, and the light source direction. We experimentally used 3–6% of the image size as the width of the stripe pattern, and adopted a process

of refinement of surface orientation for planar regions using longer line segments and wider stripe intervals.

<3> f *vs.* P_s : Fig. 11 shows $E_p^{\max}$ at image position x_i=128 (the rightmost part of the image) when we change the focal length (f=512n pixels, n=1,16) and the source direction ($\cot^{-1}(P_s)$=1+3m, m=0,15). In this figure, the source direction seems not to have a large effect on $E_p^{\max}$ although $E_p^{\max}$ is inversely proportional to the focal length as described in <1>. The source direction is, however, a very important factor because it determines the effective visual field. If we used a large incident angle between the optical axis and the source direction, the range of observable surface normals would be small.

<4> (P_o,Q_o) : Finally, we estimate the total error angle E_{space}, the difference between the true orientation (P_o,Q_o) and the estimated orientation (P_e,Q_e) in space. P_e is an average of P_l and P_r, and Q_e is estimated from P_l, P_e and the slope of the stripes in the image, which is calculated in the same central projection system as in Fig. 9. Obviously, E_{space} has its maximal value $E_{space}^{\max}$ at the four corners of the image, which are the farthest locations from the image center. Figs. 12 show the change of $E_{space}^{\max}$ at image position (128,128) for various object orientations: $-63.5^\circ < \tan^{-1}(P_o) < 63.5^\circ$, and $1^\circ < \tan^{-1}(Q_o) < 64^\circ$. (We need not consider negative Q_o because it is symmetric about the origin since we assume Q_s=0.) Figs. 12 (a), (b), (c) and (d) are for incident angles of 5, 10, 15 and 20 degrees, respectively, between the optical axis and the source direction. It is evident from these figures that the source direction has a very important role in determining the observable and measurable field of surface normals. Outside this

field, the calculated surface orientations would have serious errors.

5. DISCUSSION

We have described an algorithm which determines surface shape by projecting a stripe pattern and have evaluated the error in surface orientation introduced by assuming orthographical projection. Utilizing the results of the error estimation, we can compensate for the calculated surface orientations when the focal length is not very large. Since the location of the stripe edge points is another important factor in accurate estimation of surface orientation, as mentioned above, it is necessary to examine the effects of surface orientation, surface albedo and light source direction on edge location.

Acquisition of range information is possible in part if we utilize the results of segmentation of the 2(1/2)D image into planar or singly curved surfaces. Sugihara [11] obtains not only surface orientation but depth information by projecting stripe patterns from two different directions. Stockman and Hu [6] try to label the grid patterns using physical constraints on the scene in order to get range information. In these methods, the obtained scene features are too sparse to segment the input image into meaningful regions or to determine the parameters of surface properties. The results of segmentation using our method can be used for labeling the stripe pattern inside each region, from which we can reconstruct relative depth information at the stripe edge points. Moreover, we can easily interpolate the depth information between stripe edge points because the surface of each region has been identified as planar or singly curved in the seg-

mentation process. Figs. 13(a), (b) and (c) show the results of depth reconstruction of regions 1, 2 and 3 in Fig. 9, respectively. The depth computation is easy since we assume orthographical projection. The standard deviations of range are 0.5 pixels for the planar surfaces (region 1 and 3) and 0.7 pixels for the cylindrical surface (region 2). The variation of reconstructed range on the surfaces in Figs. 12 is due to the difference of surface albedo between the plaster used for registration of the stripe pattern and the objects, which are made from wood and painted red (cylinder) or blue (wedge). However, we cannot reconstruct the depth relation between two regions unless there is no abrupt change in depth which causes a break in the stripe pattern between these regions.

Shadow information can be a cue to extracting the depth relation between two regions which are discontinuous in depth. Using the projections of the light lines onto the image plane, which are equivalent to the epipolar lines in stereo vision, we can label each stripe in the image of two surfaces as shown in Fig. 14. This displays the upper surface of the wedge and its shadow on the back wall in Fig. 5 (a). The relative distance between them can be obtained from the equations of the light stripes in the scene. The physical constraints on the shadow, the number of stripes in the scene and the surface continuity might not be sufficient for the unique labeling of the light stripes, but can reduce the number of candidates, so that some 3-D structure of the scene can be calculated from the results of consistent labeling.

Acknowledgements

The first author wishes to thank Dr. Azriel Rosenfeld and Dr. Larry Davis for their helpful comments and discussions.

REFERENCES

[1] M. Brady, "Computational approach to image understanding," *Computing Surveys*, **14**, pp. 4–71, 1982.

[2] D. Marr and T. Poggio, "A computational theory of human stereo vision," *Proc. Royal Society of London*, **B204**, pp. 301–328, 1979.

[3] G. Xu, S. Tsuji, and M. Asada, "Coarse-to-fine control strategy for motion stereo pairs", *Proc. 9th IJCAI*, pp. 892–894, 1985.

[4] Y. Ohta and T. Kanade, "Stereo by intra- and inter-scanline search using dynamic programming," *IEEE Trans.*, **PAMI-7**, pp. 139–154, 1985.

[5] M. Yachida, S. Tsuji, and X. Huang, "WIRESIGHT: a computer vision system for 3-D measurement and recognition of flexible wire using cross-stripe light," *Proc. 6th ICPR*, pp. 220–222, 1982.

[6] G. Stockman and G. Hu, "Sensing 3-D surface patches using a projected grid", *Proc. CVPR*, pp. 602–607, 1986.

[7] R.C. Boles, P. Horaud and M.J. Hannah, "3DPO: a three-dimensional position and orientation system", *Proc. 1st Int. Symp. on Robotics Research*, pp. 413–424, 1983.

[8] M. Ohshima and Y. Shirai, "A scene description method using three-dimensional information," *Pattern Recognition*, **11**, pp. 9–17, 1979.

[9] M. Asada, H. Ichikawa and S. Tsuji, "Determining surface property by

projecting a stripe pattern", *Proc. 8th ICPR*, 1986.

[10] M. Asada and S. Tsuji, "Utilization of stripe pattern for dynamic scene analysis", *Proc. 9th IJCAI*, pp. 895–897, 1985.

[11] K. Sugihara, K. Okazaki, F. Kaihua, and N. Sugie, "Regular pattern projection for surface measurement", *Proc. 2nd Int. Symp. on Robotics Research*, pp. 17–24, 1984.

[12] Y.E. Wang, A. Mitiche, and J.K. Aggarwal, "Inferring local surface orientation", *Proc. 3rd Workshop on Computer Vision: Representation and Control*, pp. 96–104, 1985.

[13] M. Merickel, J. Lundgram, and T. Sorensen, "Cascade, an algorithm to reduce the effect of mixed pixels," *Proc. CVPR*, pp. 53–58, 1983.

[14] S. Ullman, *The Interpretation of Visual Motion*, M.I.T. Press, Cambridge, MA, 1979.

[15] M. Asada and S. Tsuji, "Representation of three-dimensional motion in dynamic scenes," *CVGIP*, **21**, pp. 118–144, 1983.

[16] J.-Q. Fang and T.S. Huang, "Some experiments on estimating the 3-D motion parameters of a rigid body from two consecutive image frames," *IEEE Trans.*, **PAMI-6**, pp. 545–554, 1984.

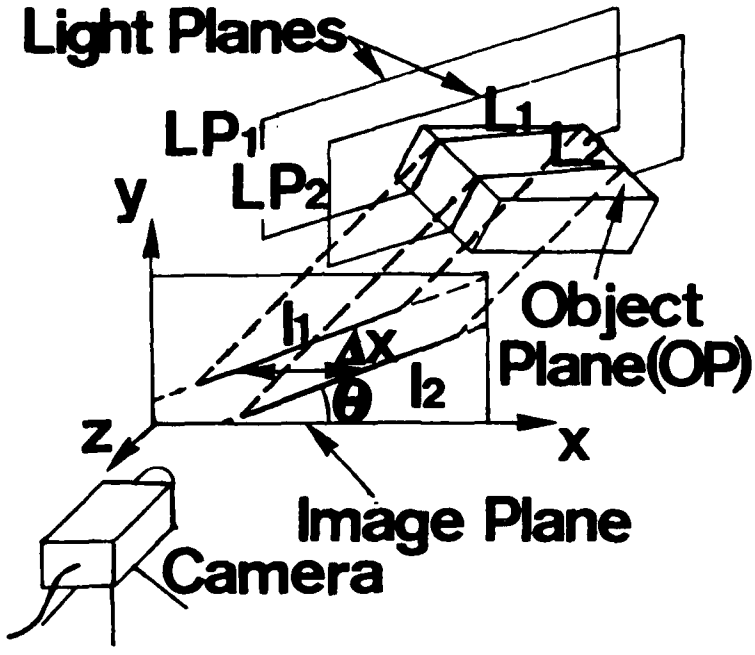

Fig. 1 System configuration

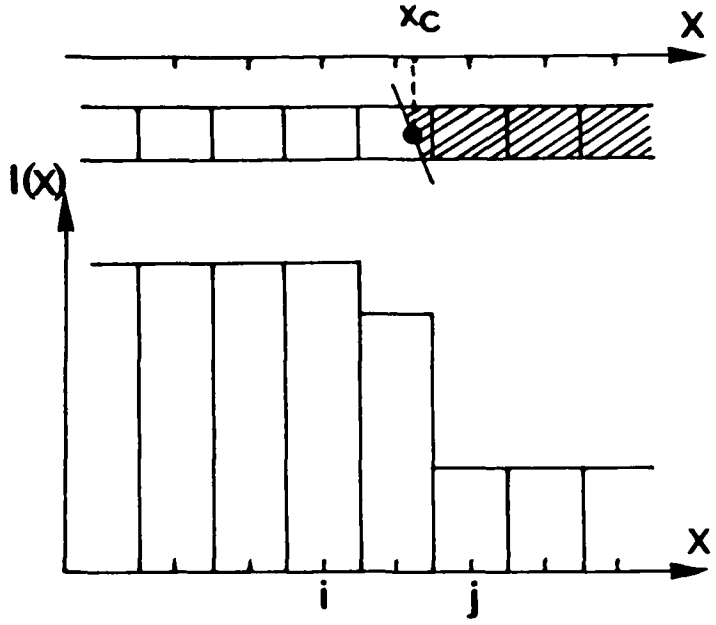

(a) A linear mixing model of image intensity $I(x)$

1	2	0	-2	-1

(b) A rectangle operator for edge detection

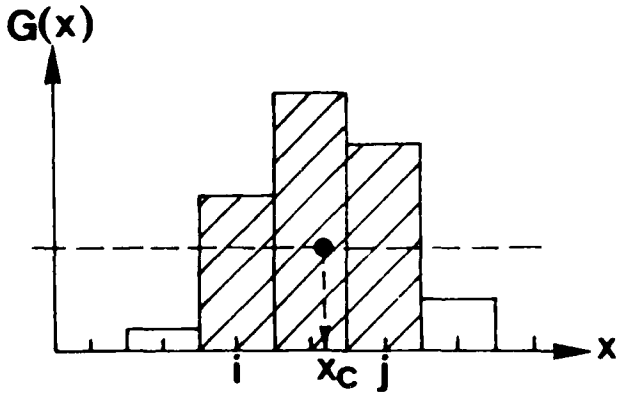

(c) Edge strength $G(x)$ obtained by applying (b) to (a)

Fig. 2 Determination of edge location

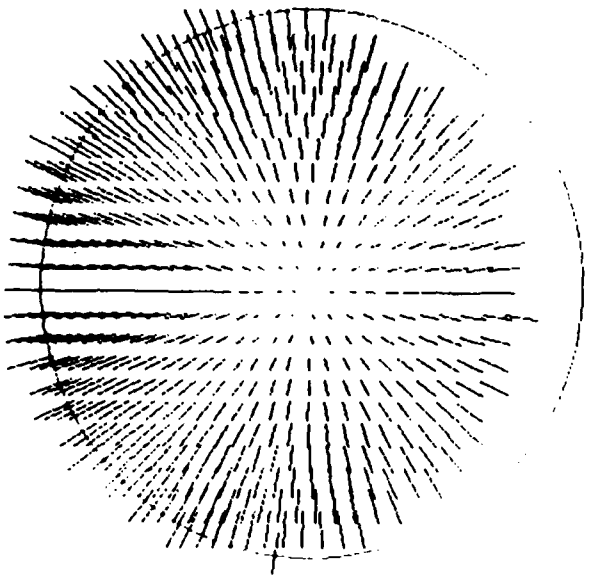

(a) Surface normals used for registration

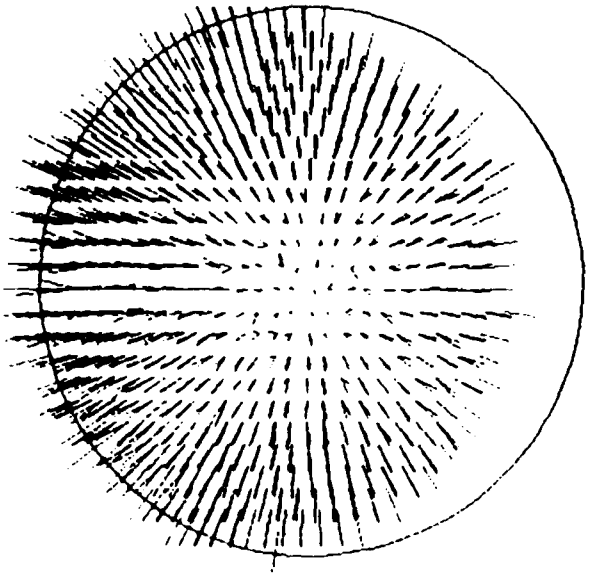

(b) Surface normals after registration

Fig. 3 Registration of stripe pattern

(a) Input image of cube

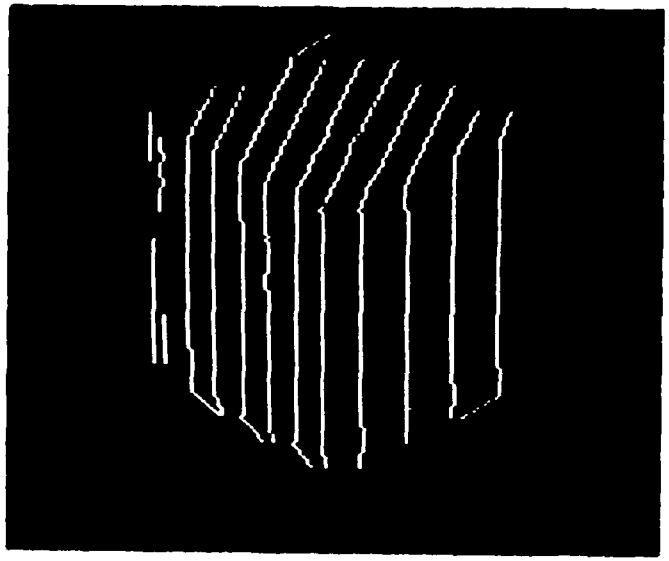

(b) Stripe edge image

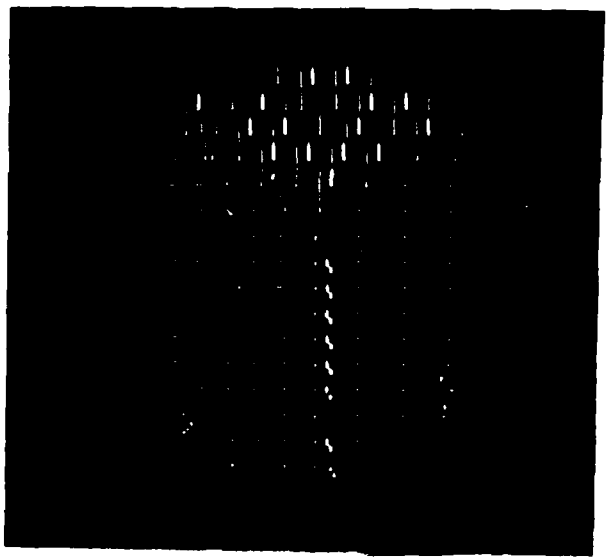

(c) Obtained surface normals

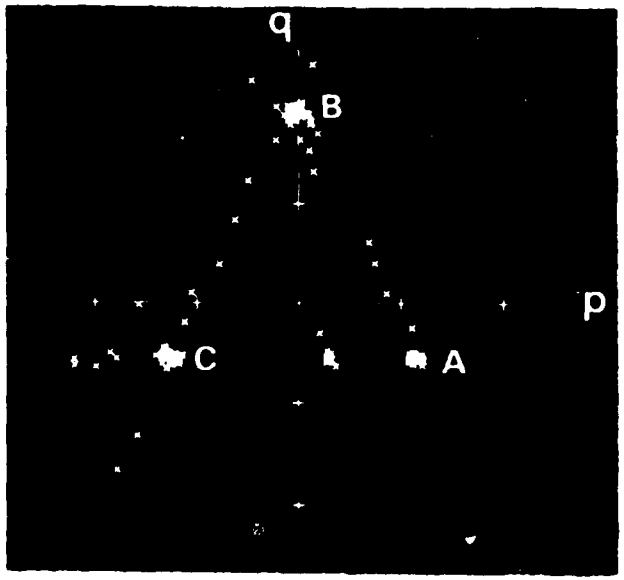

(d) Distribution of surface normals in gradient space

Fig. 4 Experimental results applied to a cube

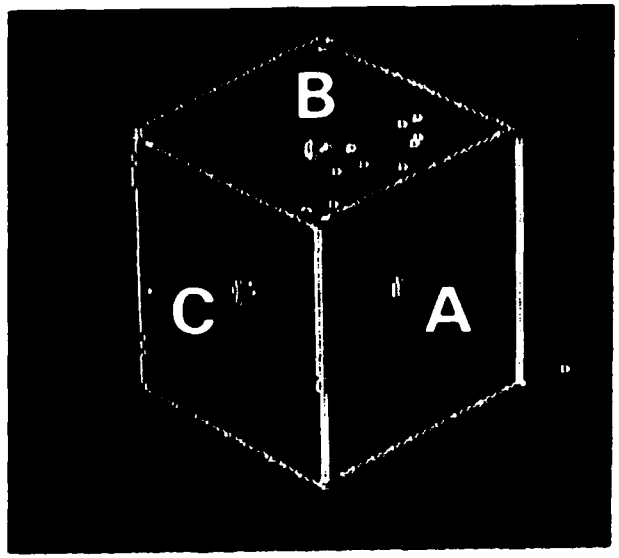

(e) Pre-segmented image

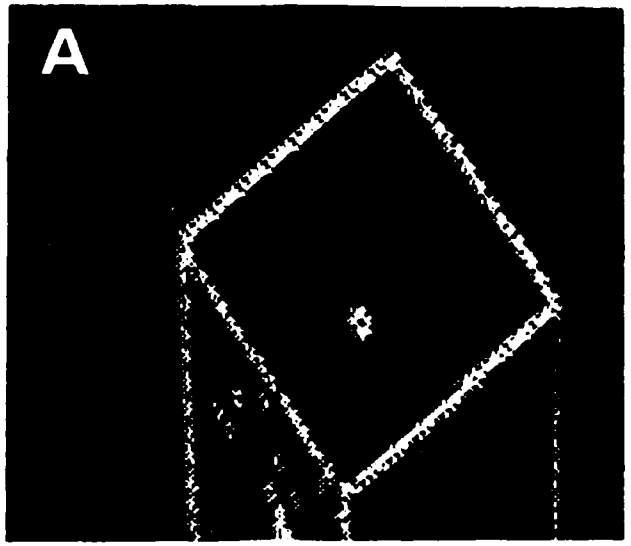

(f) Frontal view of A

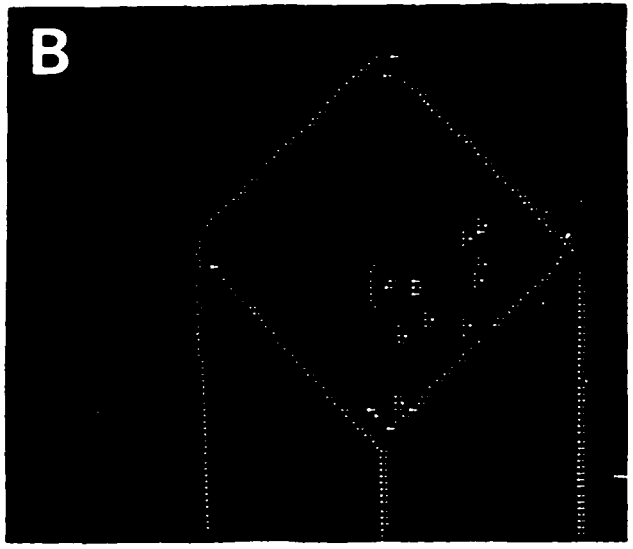

(g) Frontal view of B

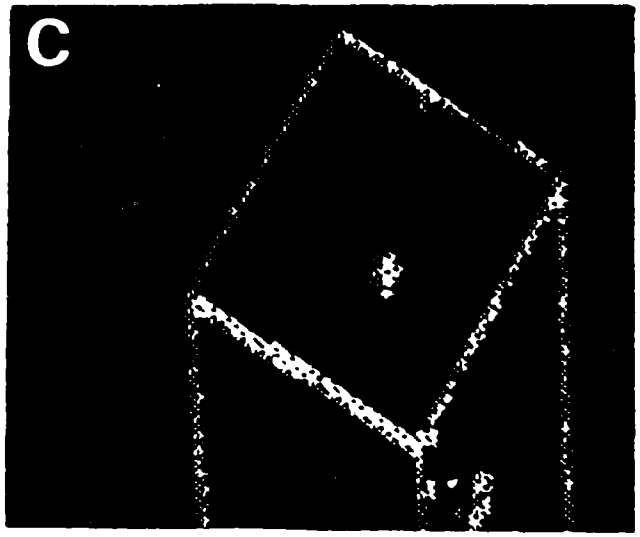

(h) Frontal view of C

Fig. 4 Experimental results applied to a cube

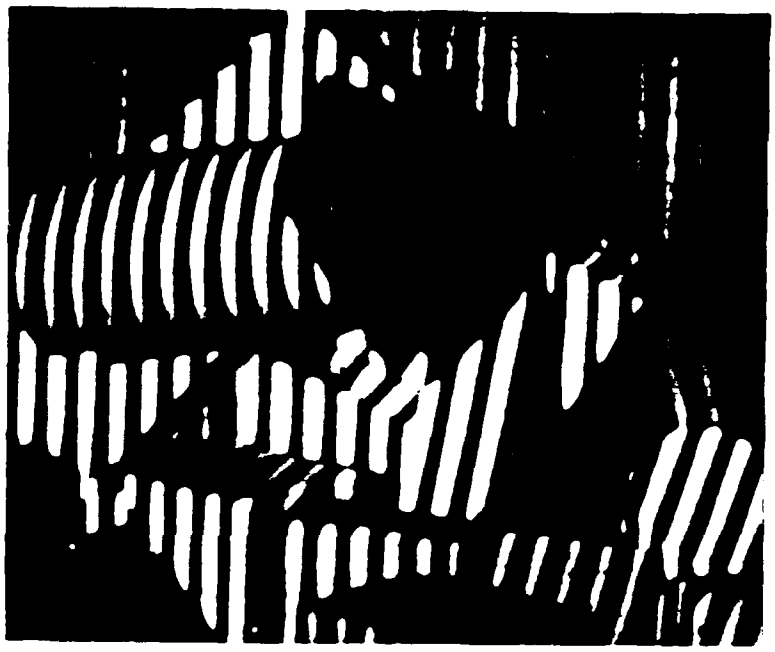

(a) The fifth frame in an image sequence

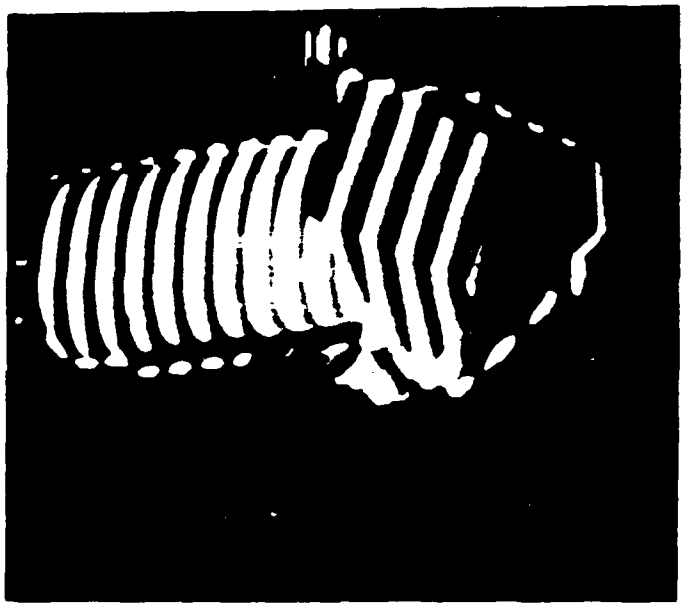

(b) Moving object in (a)

Fig. 5 Input image

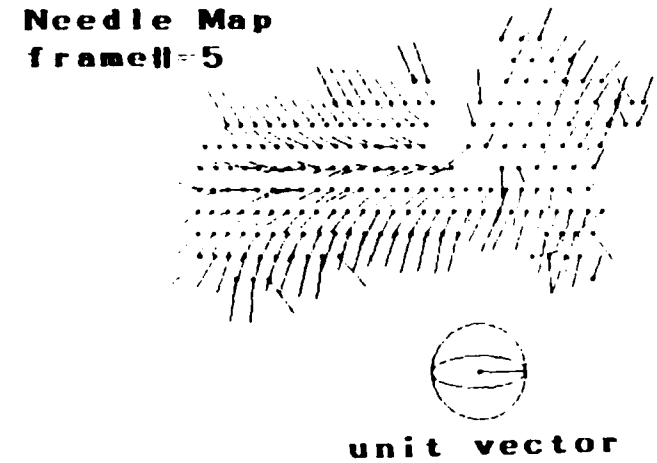

(a) Needle map of surface normals

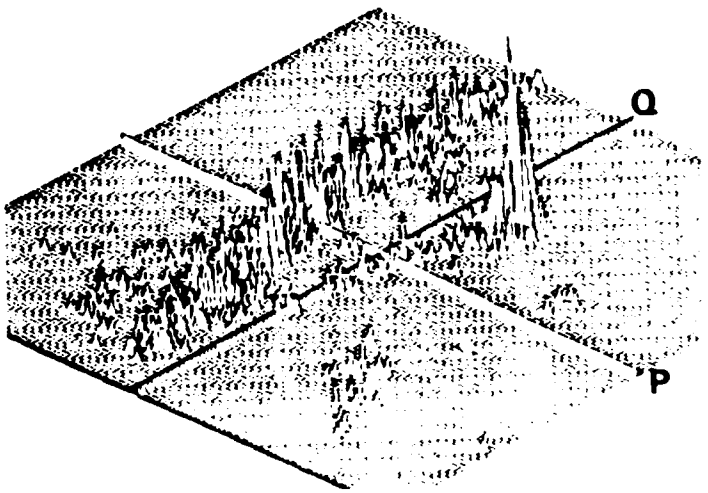

(b) Histogram of (a) in gradient space

Fig. 6 Obtained surface normals

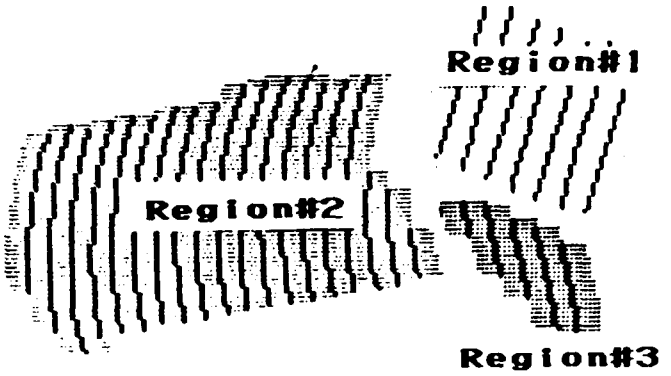

(a) Region map

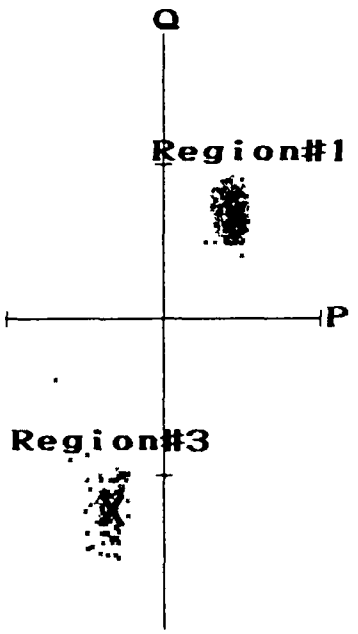

(b) Planar surfaces in gradient space

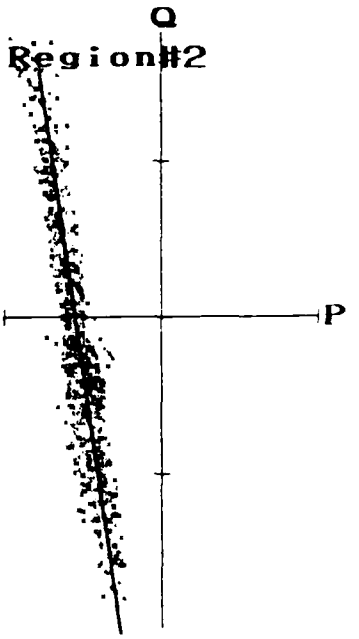

(c) Cylindrical surface in gradient space

Fig. 7 Results of segmentation

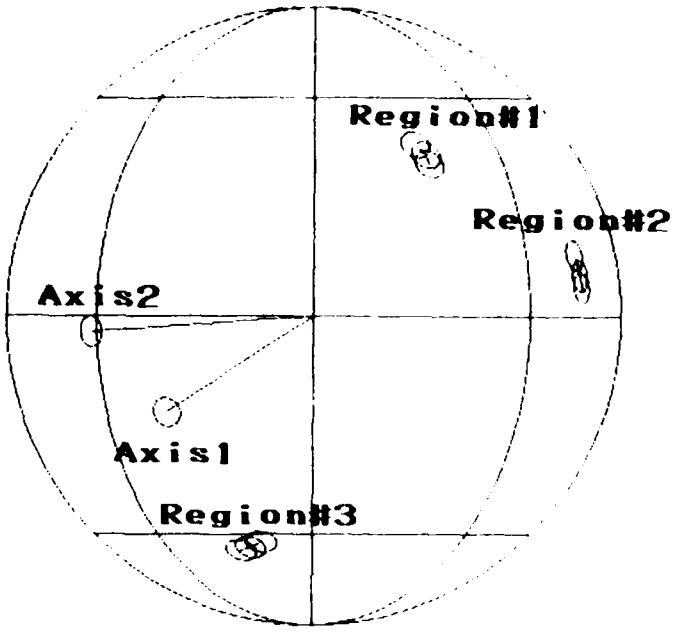

Fig. 8 Changes of surface orientation and rotation axes

Table 1. Angles between the obtained surfaces

Frame# / Region#	2	4	5	8	Mean	S. D.
1 & 2	40. 1	40. 9	40. 9	41. 4	40. 8	0. 47
2 & 3	87. 6	89. 7	88. 1	88. 7	88. 5	0. 78
3 & 1	87. 4	89. 5	88. 6	88. 8	88. 6	0. 76

(degree)

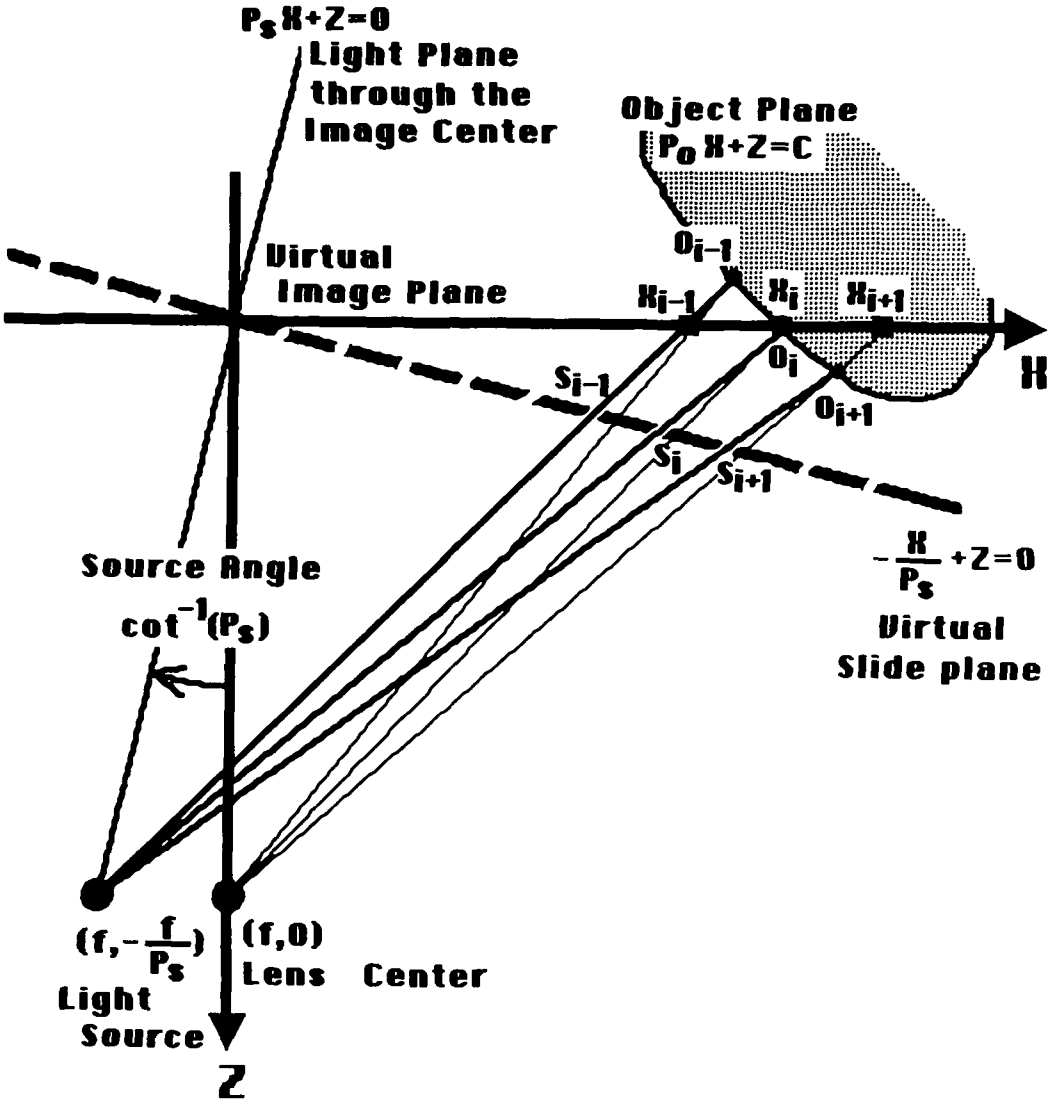

Fig. 9 Top view of image acquisition system in the central projection

Table 2. Error angle in orientation II ($D_2 - D_1$)

Width	Image Position								
(pixels)	-128	-96	-64	-32	0	32	64	96	128
2	4.17	3.13	2.09	1.05	-0.00	-1.05	-2.10	-3.15	-4.21
4	4.17	3.13	2.09	1.05	-0.00	-1.05	-2.10	-3.15	-4.21
8	4.17	3.13	2.09	1.05	-0.00	-1.05	-2.10	-3.15	-4.21
16	4.17	3.13	2.09	1.05	-0.00	-1.05	-2.10	-3.15	-4.21
32	4.17	3.13	2.09	1.05	-0.00	-1.05	-2.10	-3.15	-4.21
64	4.16	3.13	2.08	1.04	-0.01	-1.05	-2.10	-3.16	-4.21
128	4.15	3.11	2.07	1.03	-0.02	-1.07	-2.11	-3.17	-4.23

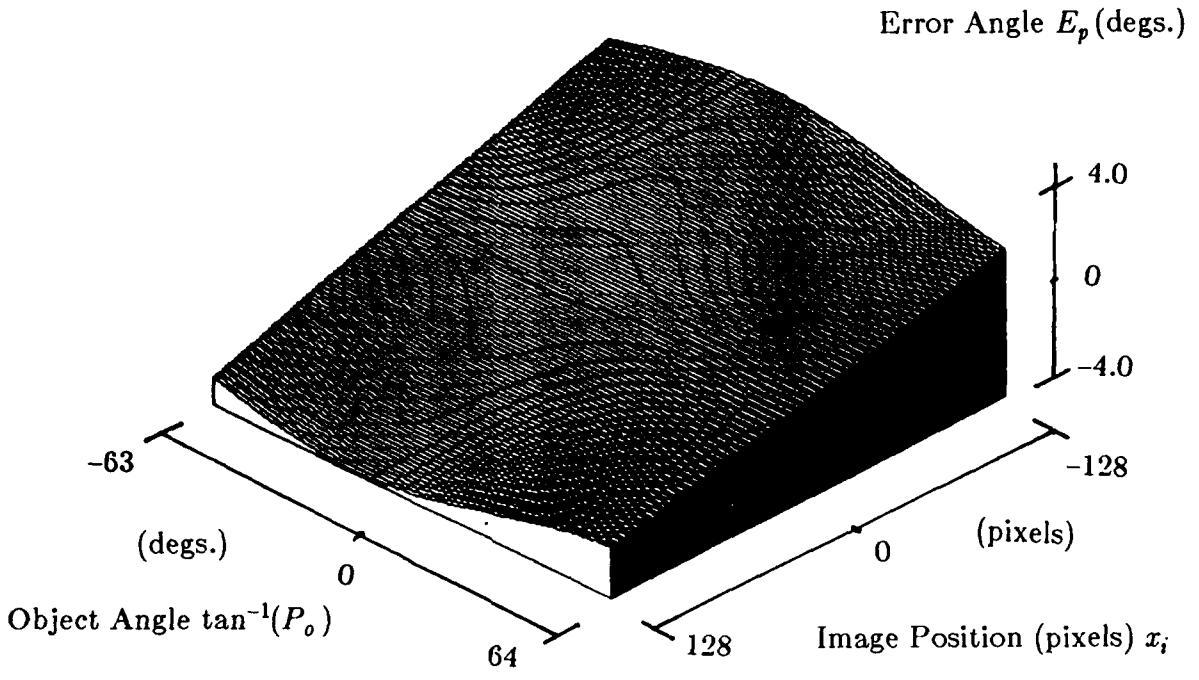

Fig. 10 Error angle in orientation I (P_o vs. $x_i(f)$)

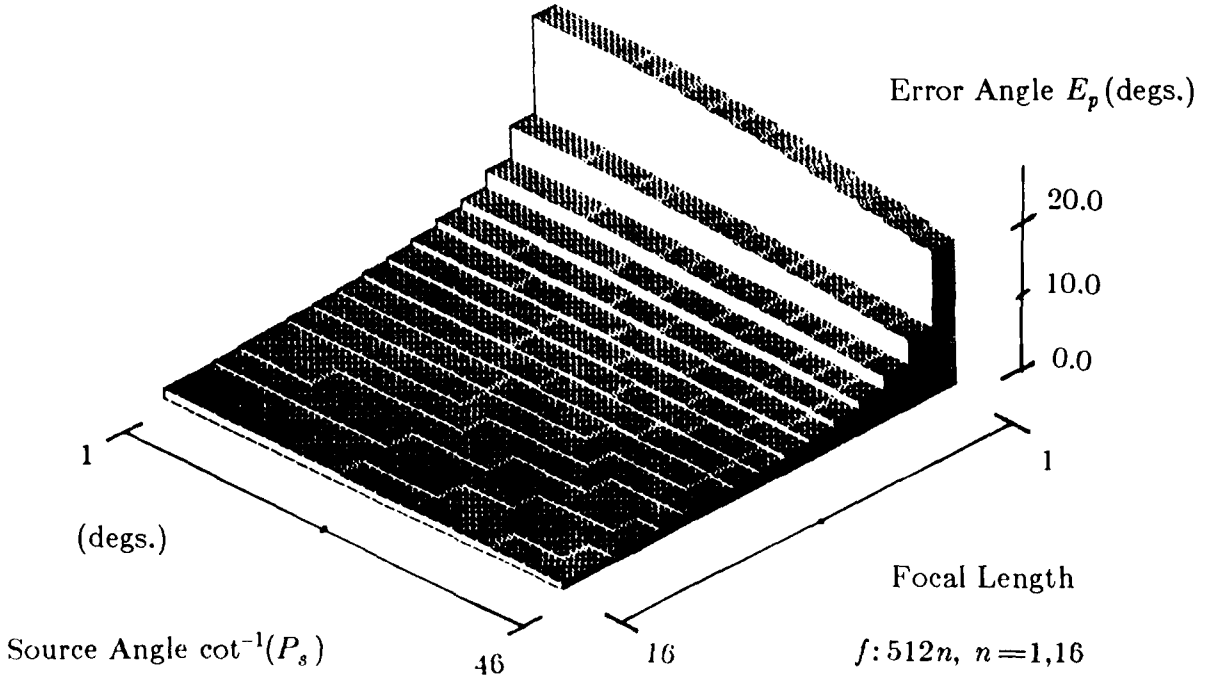

Fig. 11 Error angle in orientation III (f vs. P_s)

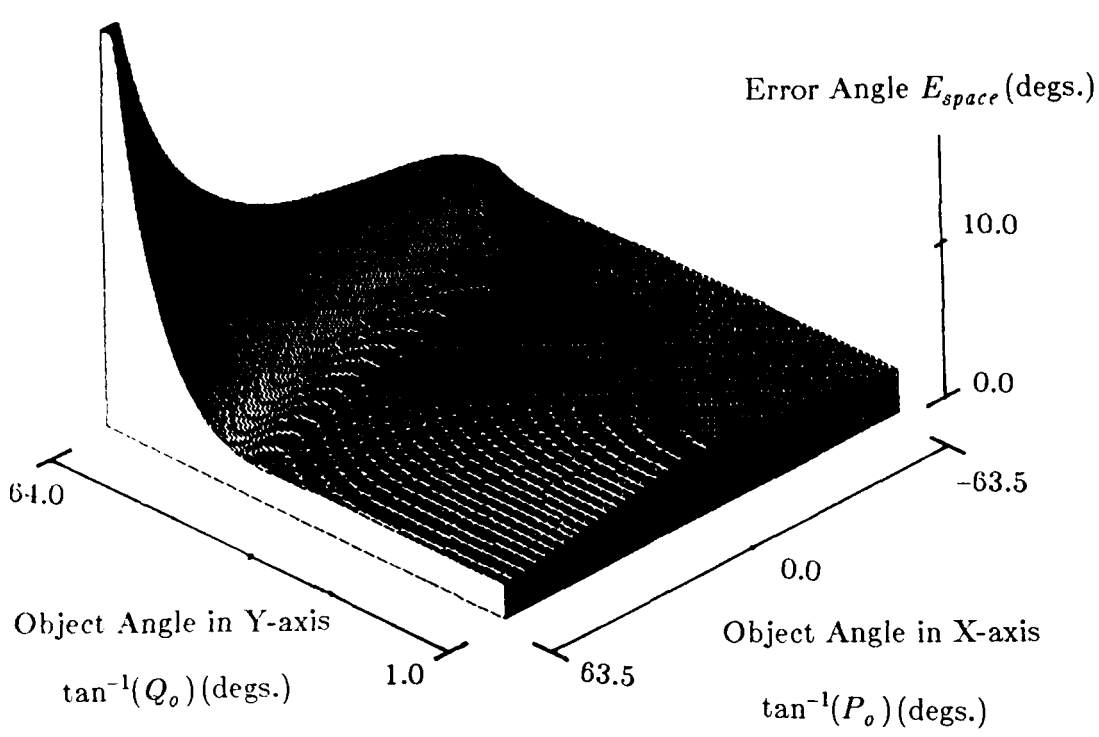

(a) Source Angle = 5 degs.

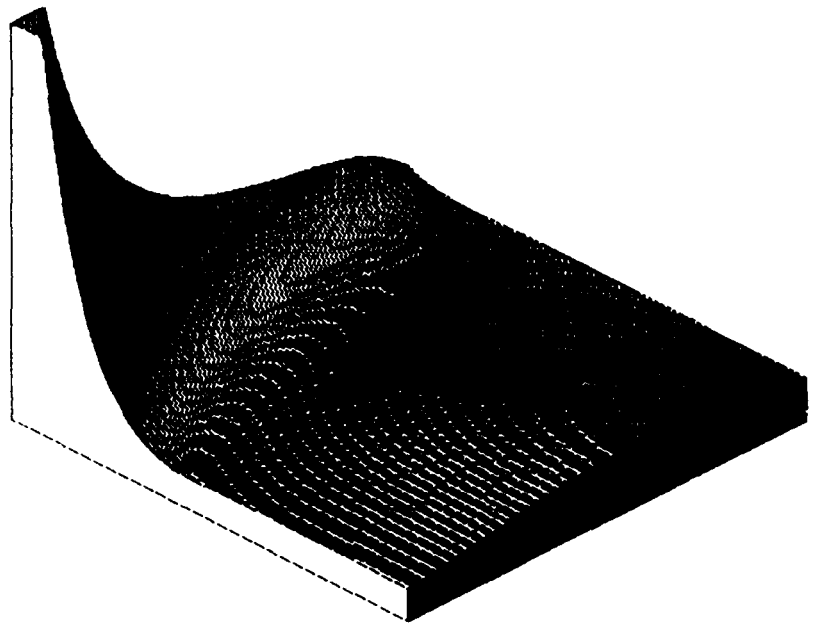

(b) Source Angle = 10 degs.

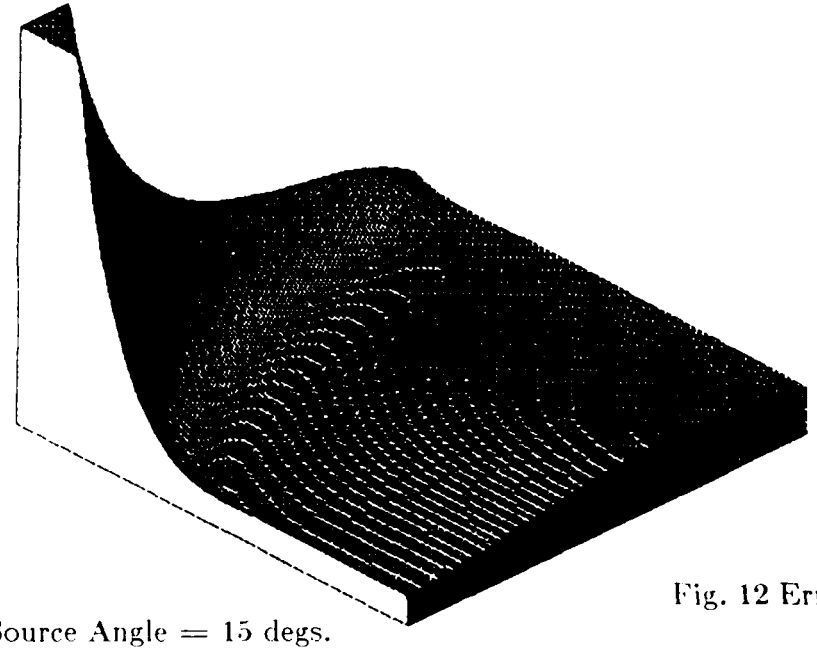

(c) Source Angle = 15 degs.

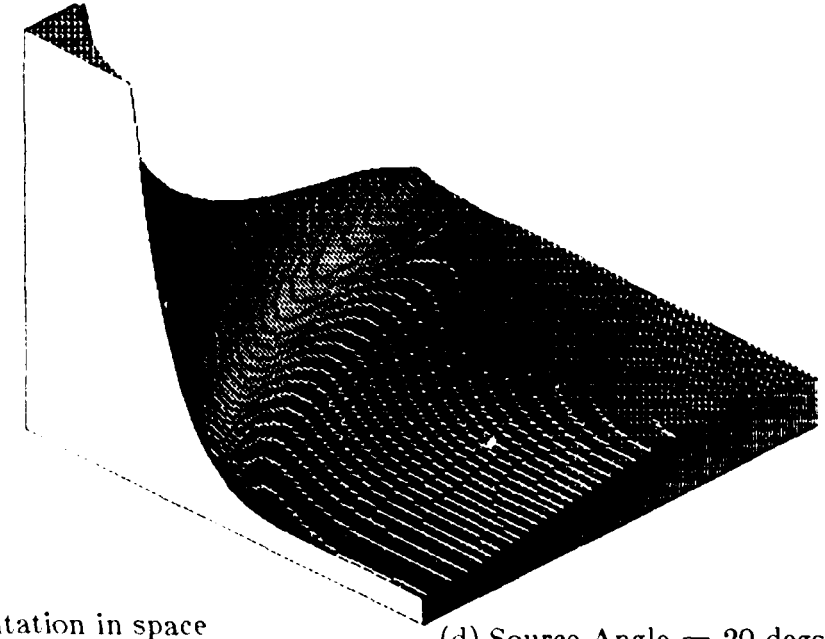

(d) Source Angle = 20 degs.

Fig. 12 Error angle in orientation in space

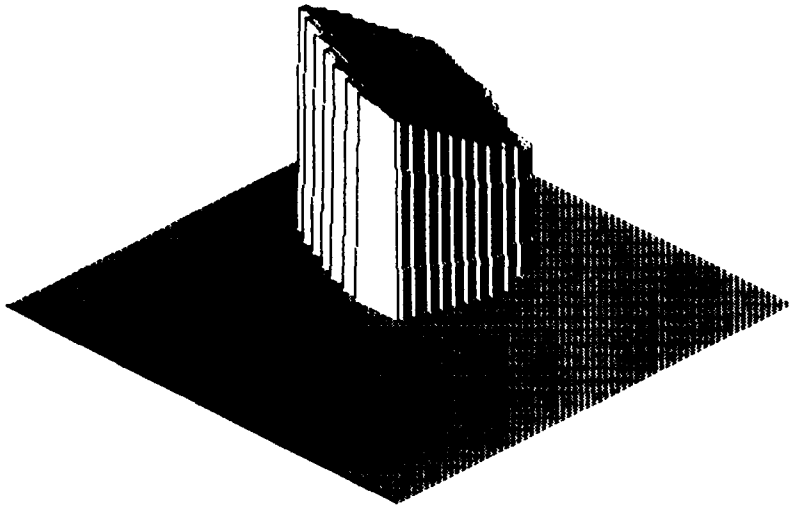

(a) Region 1

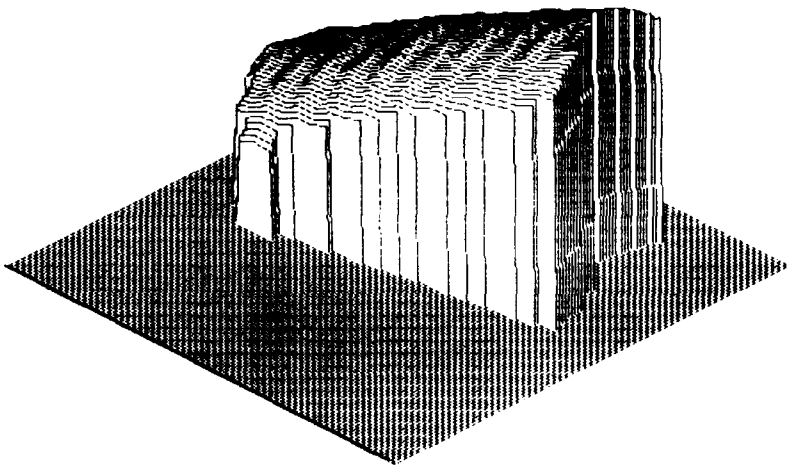

(b) Region 2

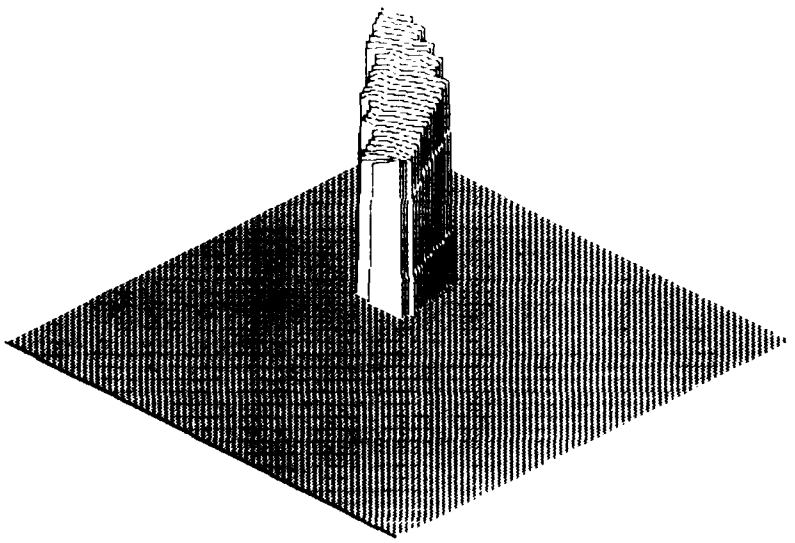

(c) Region 3

Fig. 13 Depth maps

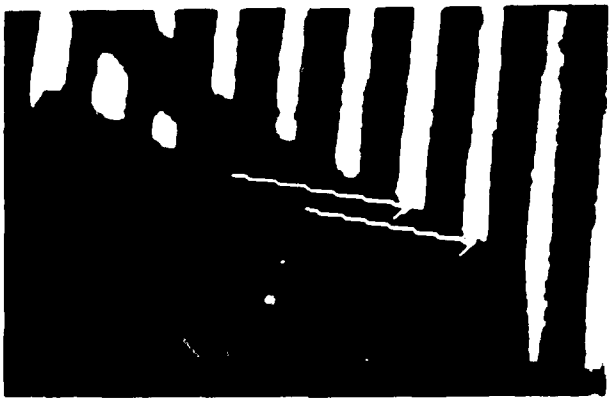

(a) Region 1

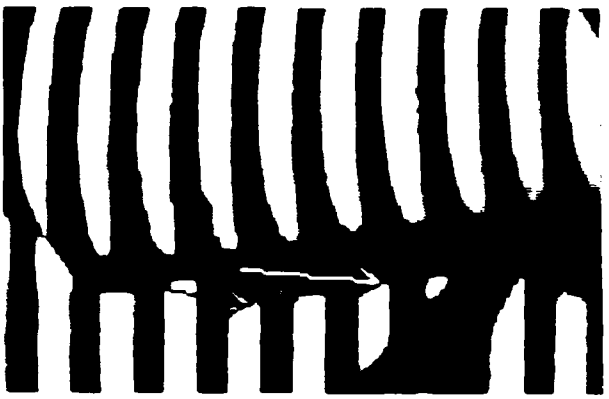

(b) Region 2

Fig. 14 Consistent labeling of stripes using shadow information

END

9-87

DTIC